Kinematical x-ray diffraction in nonuniform crystalline films: Strain and damage distributions in ion-implanted garnets

V. S. Speriosu [a)]
California Institute of Technology, Pasadena, California 91125

(Received 23 March 1981; accepted for publication 22 June 1981)

A kinematical model for general Bragg case x-ray diffraction in nonuniform films is presented. The model incorporates depth-dependent strain and spherically symmetric Gaussian distribution of randomly displaced atoms. The model is applicable to ion-implanted, diffused, and other single crystals. Layer thickness is arbitrary, provided maximum reflecting power is less than ~6%. Strain and random displacement (damage) distributions in He^+-implanted Gd, Tm, Ga:YIG, and Ne^+-implanted $Gd_3Ga_5O_{12}$ are obtained by fitting the model to experimental rocking curves. In the former crystal the layer thickness was 0.89 μm with strain varying between 0.09 and 0.91%. In the latter crystal a wide range of strain and damage was obtained using successively higher doses. In each case layer thickness was 1900 Å, with 2.49% strain corresponding to 0.40-Å standard deviation of random displacements. The strain distributions were strictly linear with dose. The same, closely linear relationship between damage and implantation-induced strain was determined for both crystals.

PACS numbers: 61.10. – i, 61.70. – r, 61.70.Tm

I. INTRODUCTION

Bragg case x-ray diffraction is a well-established method for characterizing crystalline properties of films obtained by various growth techniques. The diffracted intensity profiles (rocking curves) are highly sensitive to depth-dependent strain and damage distributions as well as lateral variations, but much of the information available in the rocking curves is generally not extracted. Part of the difficulty is due to lack of phase detection, which precludes direct inversion of the rocking curve. The remaining difficulty is the complexity of the dynamical theory of diffraction in nonuniform crystals.[1–3] At the cost of long computation time, strain profiles in diffused[4–6] and ion-implanted[7] layers were obtained by fitting dynamical theory calculations to experimental rocking curves.

The kinematical theory for symmetric reflections,[8] which involves much simpler mathematics, has offered a considerable reduction in computation time. The application[9] of the Patterson series[10] to this theory yielded parameters such as mean strain, damage, and layer thickness. In another approach, detailed strain and damage distributions were obtained by fitting a kinematical theory model to rocking curves of successively etched samples.[11,12] However, both approaches were limited to symmetric reflections which provide a limited amount of information.

In this paper a general Bragg case kinematical expression for the reflecting power of nonuniform films is obtained from the uniform single-crystal dynamical theory.[13] Depth-dependent strain distributions are represented by a set of independently but coherently diffracting laminae oriented parallel to the surface. Each lamina incorporates many unit cells and has uniform strain. In addition to coherent atomic displacements, random displacements (damage) are treated through their effect on the mean structure factor in each lamina. The range of validity of the kinematical approximation is shown to include most cases of technological importance. The relative sensitivity to strain, damage, and layer thickness is demonstrated. Using this model, strain and damage distributions are obtained by fitting rocking curves of He^+-implanted Gd, Tm, Ga:YIG, and Ne^+-implanted gadolinium gallium garnet (GGG). In the former crystal three different strain and damage distributions were created by single and multiple implantations. Rocking curves of symmetric and asymmetric reflections were fitted. The latter crystal was implanted with single doses resulting in a wide range of strain and damage. Symmetric reflection rocking curves corresponding to each dose were fitted.

II. THE KINEMATICAL MODEL

The plane-wave dynamical theory[13] predicts that for unit electric-field amplitude incident on the surface of an isolated, uniform, nonabsorbing, single-crystal plate, the diffracted amplitude at the same surface is

$$E_D = e^{-i2\pi(\mathbf{K}_0^e + \mathbf{B}_H)\cdot\mathbf{r}} D_D, \tag{1}$$

$$D_D = i\,\frac{F_H}{|F_H|}\sqrt{|b|}\times\frac{\sin\left[A\,(Y^2-1)^{1/2}\right]}{(Y^2-1)^{1/2}\cos\left[A\,(Y^2-1)^{1/2}\right]+iY\sin\left[A\,(Y^2-1)^{1/2}\right]}, \tag{2}$$

where the following definitions apply: $\mathbf{K}_0^e$ = incident external wavevector, $|\mathbf{K}_0^e| = 1/\lambda$, $\mathbf{B}_H$ = reciprocal lattice vector, $\mathbf{r}$ = vector from origin (chosen on the surface), F_H = structure factor, $b = \gamma_0/\gamma_H$; γ_0, γ_H are direction cosines of incident and diffracted wavevectors, respectively, from the inward normal to the surface;

$$A = \frac{e^2}{mc^2}\,\frac{\lambda\,|F_H|}{V}\,\frac{t}{(|\gamma_0\gamma_H|)^{1/2}}, \tag{3}$$

where e^2/mc^2 = classical electron radius, V = volume of

[a)]IBM predoctoral fellow.

 0021-8979/81/106094-10$01.10

unit cell, t = plate thickness,

$$Y = \frac{[(1-b)/2]\psi_0 + (b/2)\alpha}{(\sqrt{|b|})|\psi_H|}, \tag{4}$$

$$\psi_{0,H} = -\frac{e^2}{mc^2}\frac{\lambda^2}{\pi}\frac{F_{0,H}}{V},$$

$$\alpha = -2\Delta\theta \sin 2\theta_B,$$

$$\Delta\theta = \theta - \theta_B,$$

θ_B = Bragg angle.

Equations (2)–(4) are valid only for σ polarization. For π polarization F_H is replaced by $F_H \cos 2\theta_B$.

If the plate thickness and/or the structure factor are sufficiently small, corresponding to $A \ll 1$, Eq. (2) reduces to the kinematical limit:

$$D_K = i\frac{F_H}{|F_H|}(\sqrt{|b|})e^{-iAY}\frac{\sin(AY)}{Y}. \tag{5}$$

Equations (3) and (4) apply to unstrained and undamaged lattice. If the lattice is strained in a direction perpendicular to the sample surface, the corresponding change in Eq. (4) is

$$\Delta\theta \rightarrow \Delta\theta + \epsilon^{\perp}[|\gamma_H|(1-\gamma_H^2)^{1/2} + \gamma_H^2 \tan\theta_B]. \tag{6}$$

Here $\epsilon^{\perp}$ is the strain and the correction includes changes in the direction and magnitude of the reciprocal lattice vector. Equation (6) can be easily extended to include lateral strain. However, the requirement of lattice match between film and substrate generally does not allow lateral strain.

In ion-implanted crystals, a significant fraction of atoms may be displaced from lattice positions. The statistical distribution of displacements $\Delta\mathbf{r}_j$ away from lattice j is described by a function $\rho(\Delta\mathbf{r}_j)$. Such a distribution will result in a mean structure factor

$$\langle F_H \rangle = \sum_j f_j \int d^3r \rho(\Delta\mathbf{r}_j) e^{-i2\pi\mathbf{B}_H\cdot(\mathbf{r}_j + \Delta\mathbf{r}_j)}, \tag{7}$$

where f_j is the atomic scattering factor for site j, located at $\mathbf{r}_j$ in undamaged crystal. If the same spherically symmetric Gaussian form is assumed for all sites, the mean structure factor becomes

$$\langle F_H \rangle = \exp\left(-\frac{8\pi^2}{\lambda^2}\sin^2\theta_B U^2\right)F_H^0 = e^{-W}F_H^0, \tag{8}$$

where F_H^0 corresponds to undamaged crystal and U is the standard deviation of displacements. This correction to F_H^0 is the well-known Debye-Waller factor.[13] Its form can be readily modified for other $\rho(\Delta\mathbf{r}_j)$ distributions, but, for simplicity, in this paper a spherically symmetric Gaussian $\rho(\Delta\mathbf{r}_j)$ is assumed.

Strain and damage distributions are represented by a set of discrete laminae oriented parallel to the surface. Each lamina contains a large number of unit cells, but is sufficiently thin so that extinction[13] and normal absorption within the lamina are negligible. Each lamina has its own uniform strain $\epsilon^{\perp}$ and random displacement standard deviation U. Dynamical interactions among different laminae are neglected, as is the effect of extinction on the incident wave. The total diffracted amplitude is then the sum of coherently interfering functions of the type shown in Eq. (5), adjusted for phase lags and normal absorption during traversal through the crystal. Although usually extinction is stronger than normal absorption,[13] for depth-dependent strain distributions the latter can be more important. With these considerations, the total amplitude from N laminae is

$$E_N = i\frac{F_H}{|F_H|}(\sqrt{|b|})\sum_{j=1}^{N} a_j e^{-i(A_jY_j+\phi_j)}\frac{\sin(A_jY_j)}{Y_j}, \tag{9}$$

where

$$a_j = \exp\left[-\mu\frac{\gamma_0 + |\gamma_H|}{2|\gamma_0\gamma_H|}\sum_{i=j+1}^{N} t_i\right]; \quad a_N = 1,$$

$$\mu = \frac{2\lambda}{V}\frac{e^2}{mc^2}\,\mathrm{Im}(F_0),$$

t_i = thickness of lamina i,

$$\phi_j = 2\sum_{i=1}^{j-1} A_i Y_i; \quad \phi_1 = 0,$$

and the previously defined variables Y and A are now subscripted to indicate dependence on strain and damage. In addition, since Eq. (9) will be used to determine strain relative to virgin crystal, the refraction correction $[(1-b)/2]\psi_0$ in the definition of Y [Eq. (4)] is neglected.

In principle the total amplitude due to laminar structure and substrate is

$$E_T = E_N + a_1 e^{-i2A_1Y_1}E_s, \tag{10}$$

where E_s is the dynamical result for a thick, aborbing, perfect crystal. However, the observed rocking curves of thick, supposedly uniform crystals are frequently broader than predicted for perfect crystals. The discrepancy is due to lattice parameter variations and, to a lesser extent, Compton and thermal diffuse scattering. For the purpose of fitting rocking curves of thin surface layers, the discrepancy in the substrate intensity can be removed by using a function which matches it in the angular range of interest. In addition, the relatively wide substrate peak implies that its amplitude does not have a well-defined phase. Therefore, the total calculated intensity should be only the sum of layer and substrate intensities. The total reflecting power is

$$R_T = \frac{1+\cos^4 2\theta_B}{1+\cos^2 2\theta_B}\frac{|\gamma_H|}{\gamma_0}E_N E_N^* + R_s, \tag{11}$$

where the first factor represents the relative abundance of σ- and π-polarization in double-crystal diffractometry, $|\gamma_H|/\gamma_0$ relates intensity to power, and R_s is the substrate reflecting power.

Because of the approximations made in arriving at Eq.(11), it cannot be indiscriminately applied to films of arbitrarily large thickness. As thickness increases, particularly if the strain distribution is constant, dynamical effects become dominant. It is therefore important to consider the range of validity of the kinematical theory. For constant strain and $A \lesssim 0.25$, the kinematical [Eq. (5)] and dynamical [Eq. (2)] amplitudes are in extremely close agreement. The upper limit corresponds to about 6% reflecting power. For $0.25 \lesssim A \lesssim 1$, the kinematical expression yields a sharper and more peaked curve, but the discrepancy is not more than

$\sim 15\%$. Choosing 6% reflecting power as the upper limit of validity and considering only the strongest reflections, the corresponding layer thickness is 2000 – 4000 Å for crystals such as Si, Ge, GaAs, and magnetic garnet. This range is for constant strain. If the strain is depth-dependent, as is true of ion-implanted, diffused, and other films, the range of validity for the kinematical theory can be several times larger. Dynamical effects depend strongly on the Bragg condition, $Y = 0$, being satisfied throughout the layer; this does not happen in nonuniform films. Since the thickness for which the kinematical model is valid varies with the strain distribution, a definite upper limit cannot be given. However, the agreement with dynamical theory for $R_T \lesssim 6\%$ suggests that rocking curves with maxima up to this value can be safely interpreted kinematically. For typical distributions this value of R_T corresponds to ~ 1-μm total thickness.

III. ROCKING CURVE SENSITIVITY TO STRAIN, LAYER THICKNESS, AND DAMAGE

Expression (9) for the diffracted amplitude, taken to the integral limit, is proportional to the Fourier transform of the strain and damage distributions. However, the lack of phase detection precludes direct inversion of the rocking curve. The distributions can be obtained by fitting the rocking curve with Eq. (11) evaluated for assumed distributions. A good fit of the data is then taken to mean that the actual distributions were found. Since the validity of this assumption cannot be mathematically proved, it is useful to examine the rocking curve sensitivity to strain and damage. Figure 1(a) shows two strain distributions obtainable by He^+-implantation in garnet. The distributions are plotted versus distance from the interface with the unstrained substrate. The number of laminae is such that further subdivision does not affect the calculated rocking curve. The distributions have the same thickness but differ by $\pm 5\%$ in their detailed shapes, i.e., distribution 1 (dashed) is slightly sharper. It is assumed that there is no damage, i.e., $U_j \equiv 0$ for all laminae. The corresponding calculated rocking curves for Cu K_α (444) are shoown in Fig. 1(b). The structure in the range -0.24 deg $\lesssim \Delta\theta \lesssim -0.04$ deg is entirely due to the strain distributions of Fig. 1(a). For $|\Delta\theta| \lesssim 0.03$ deg, the substrate reflecting power, obtained from dynamical theory, is dominant.

Although rocking curves 1 and 2 are qualitatively very similar, there are large differences in the positions of their maxima and minima. The differences indicate a high sensitivity to strain distribution and furnish the confidence that a distribution yielding a good fit of the data is not only unique, but also highly accurate. The accuracy depends on the particular strain distribution, and ranges from $\pm 5\%$ to $\pm 2\%$ strain for layer thicknesses between ~ 2000 Å and ~ 6000 Å.

Similar accuracy exists for the total strained layer thickness. For uniform strain, Eq. (5) relates the thickness to the period of oscillation. For depth-dependent strain, the period is no longer constant [see Fig. 1 (b)]. For positive strain, at a given $\Delta\theta$ it roughly measures the thickness for which the strain is greater than the value obtained by setting the right side of Eq. (6) equal to zero. For example, the period between -0.06 deg and -0.03 deg yields the total layer thickness in Fig. 1(a).

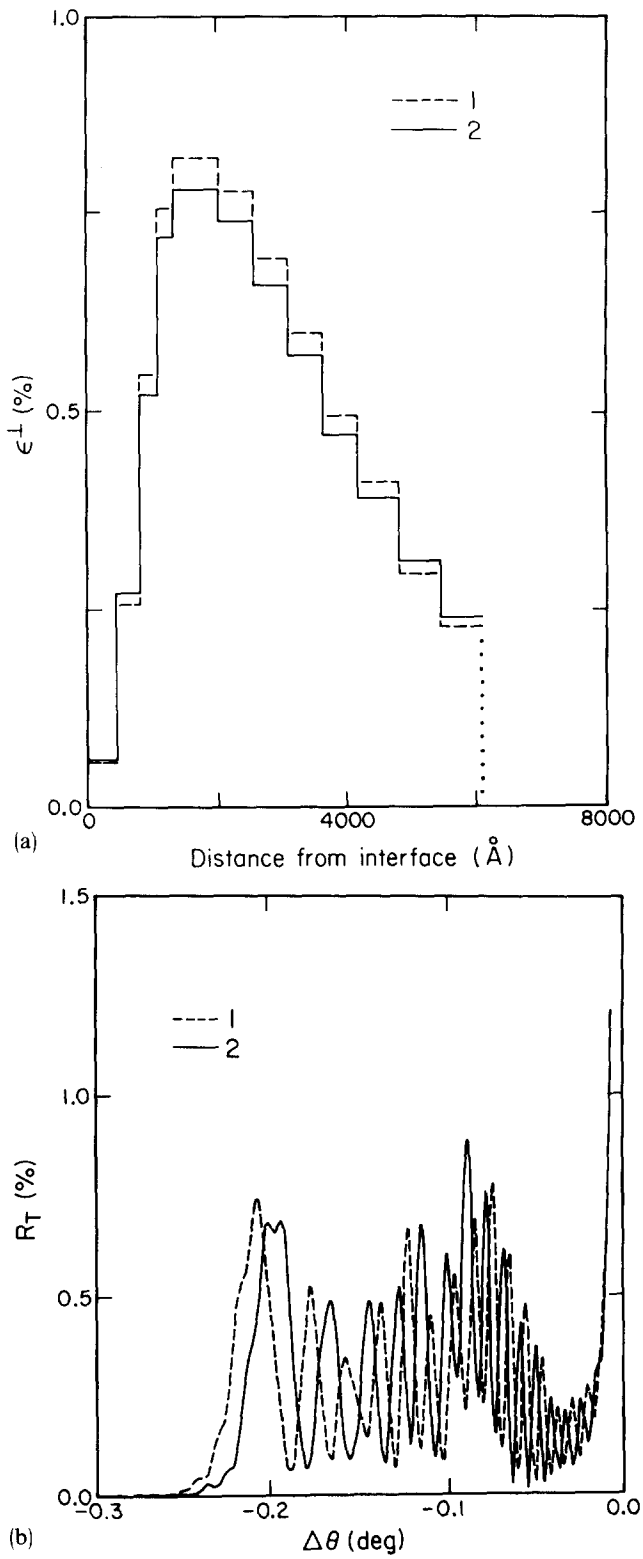

FIG. 1. (a) Strain distribution (dashed) obtainable by He^+-implantation in garnet. The solid line is a $\pm 5\%$ variation. The distributions are plotted vs distance from the interface with unstrained substrate. (b) Calculated Cu K_α (444) rocking curves corresponding to the strain distributions of Fig. 1(a). The angle $\Delta\theta$ is referred to the location of the substrate peak.

The theoretical sensitivity to the damage parameter U is considerably less than to strain and thickness. For uniform

strain and damage, the reflecting power goes as e^{-2W}, where W is proportional to U^2 [Eq. (8) and (11)]. From this

$$\Delta U \sim \frac{1}{U}\frac{\Delta R_T}{R_T} \tag{12}$$

so that for low U the relative uncertainty is quite large. At moderate to high damage levels the sensitivity improves, approaching that for strain.

IV. EXPERIMENT

A series of ⟨111⟩ Gd, Tm, Ga: YIG samples subjected to three He^+-implantation conditions was supplied by an external source.[14] The films were grown by LPE on 0.5-mm-thick Czochralski-grown ⟨111⟩ $Gd_3Ga_5O_{12}$ (GGG), were about 0.9 μm thick, and had a quoted composition $\{Gd_{0.84}Tm_{1.17}Y_{0.99}\}[Fe_2](Ga_{0.39}Fe_{2.61})O_{12}$. Implantation was done at room temperature, several degrees off ⟨111⟩ axis and with current densities of $\sim 0.1\ \mu A/cm^2$. The implantation conditions were 140 keV, 3×10^{15} He^+/cm^2 (denoted here as FI); FI + 70 keV, 1.4×10^{15} He^+/cm^2 (≡FII);FII + 30 keV, 9×10^{14} He^+/cm^2(≡FIII). According to a model[15] relating certain magnetic properties to nuclear energy loss, the three conditions should yield increasingly uniform properties with depth. For each implanation condition a series of samples was made by ion milling to successively greater depths. In addition, several duplicates of as-implanted samples were provided. The size of these samples was $\sim 4\times4$ mm^2.

As will be shown, the He^+ doses resulted in relatively low levels of damage. In order to explore the validity of the kinematical diffraction model over a wider range of damage, a series of GGG samples, provided by another source,[16] was implanted at room temperature with 100-keV Ne^+ at 0, 0.5, 1.0, 2.0, and 6.0×10^{14} atoms/cm^2. These samples will be denoted as PI through PV. The orientation, thickness, and growth-method of the virgin GGG were the same as for the magnetic film subtrates.

Double-crystal rocking curves were obtained using the appartus shown in Fig. 2. X-rays from a Cu target operated at 40 keV, 20 mA are collimated by a $\sim 0.5\times1$-mm^2 slit and undergo Bragg diffraction by the stationary first crystal. The diffracted beam is partially polarized, has a lateral divergence of not more than ~ 25 arc sec, and consists of the K_α line. The beam is then diffracted by the sample which is continuously rotated at 0.2 arc sec/sec in the neighborhood of the Bragg condition. In addition to the $\Delta\theta$ variation, the sample can be rotated in azimuth prior to measurement. In symmetric reflections this rotation provides information about sample curvature and lateral uniformity. The radiation is measured by a stationary "wide-open" Na I (Tl) detector with pulse-height analysis electronics. Typical counting rate for the beam incident on the sample was $\sim 10^5$ cps. The measured reflections were (444), (888), and (880), the latter with both asymmetries. The sample and the first crystal (a piece of ⟨111⟩ GGG) were set for the same reflection and asymmetry.

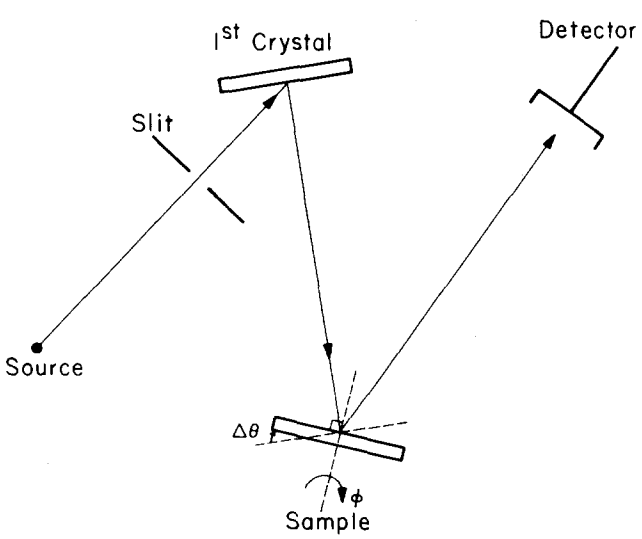

FIG. 2. Double-crystal x-ray diffraction apparatus.

V. RESULTS

A. He^+-implanted Gd, Tm, Ga:YIG

Figure 3(a) shows the experimental (dashed) and calculated (solid) rocking curves of sample FI, implanted with 140 keV, 3×10^{15} He^+/cm^2. Curves labeled 0 correspond to as-implanted material, while curves 1 and 2 are of samples which were ion milled to mechanically determined[14] depths of ~ 2500 and ~ 6800 Å, respectively. It should be noted that the curves belong to different samples cut from the same wafer. The reported uniformity of implanation across the wafer was about $\pm$ 5%. Differences in experimental rocking curves of as-implanted samples also indicate lateral variations of up to $\pm$ 5%. Unless data are taken of the same sample before and after milling, lateral variations will limit the agreement of experimental and calculated curves corresponding to different depths. Consequently the primary objective was to obtain strain and damage distributions which produce the best fit to the unmilled rocking curve. The distributions were built from the bottom up, using curves 2 and 1, together with the quoted milled depth, only as guides. Even so, the final distributions, shown in Fig. 3(b), yield rocking curves which match all three experimental curves quite well. The discrepancy in curves 1 can be removed by lowering the strain by about 5%.

Since strain is defined relative to the GGG substrate, the strain distribution [solid line in Fig. 3(b)] includes a region, 2800 Å thick, of constant strain. Its source is the lattice parameter difference between the LPE film and substrate. At greater distances from the interface, the total strain is the sum of the constant value and the implantation-induced strain. At any depth, the uncertainty in strain is not more than $\pm$ 2% of the maximum strain. The distribution [dashed in Fig. 3(b)] for the damage parameter U is linear with implantation-induced strain. That is, $U_j = 0.18\,\epsilon_j^{\perp}$, with $\epsilon_j^{\perp}$ in percent and U_j in Å. Because of the relatively large uncertainity ($\pm$ 15%) in U at this damage level, some deviation from linearity cannot be ruled out. However, the average U is determined by closely matching the integrated experimental reflecting power $\int R_T d(\Delta\theta)$. In addition, the details of the rocking curves are best simulated by similar $\epsilon^{\perp}$

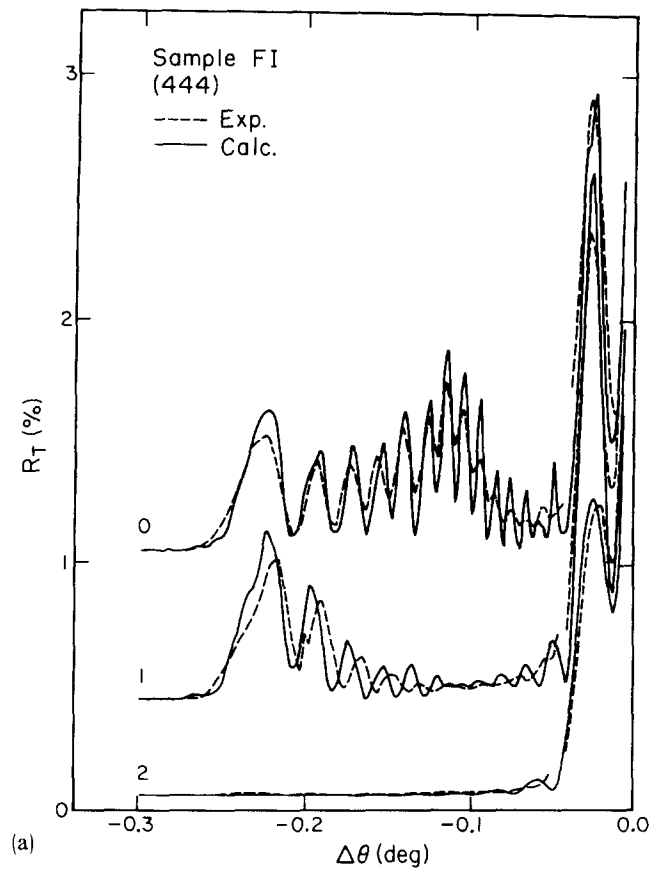

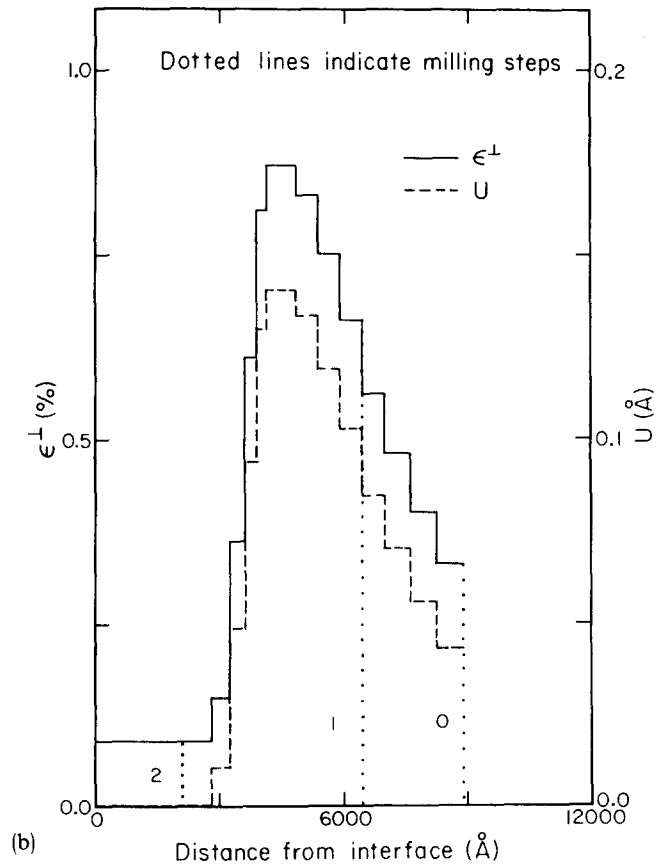

FIG. 3(a) Experimental (dashed) and calculated (solid) (444) rocking curves of sample FI (140 keV, 3×10^{15} He^{+}/cm^{2}). Curve 0 is from unmilled material; curves 1 and 2 correspond to progressively deeper milling. The curves are vertically displaced for clarity. (b) Strain (solid) and damage parameter U (dashed) distributions in sample FI. The vertical dotted lines indicate milling steps and are labeled to show correspondence with the data of (a).

and U distributions. In particular, the maximum $\epsilon^{\perp}$ and the maximum U occur at the same depth.

Rocking curves of sample FI (unmilled), obtained with (888) and (880) reflections, are shown in Fig. 4 and 5(a). Both curves are qualitatively similar to the (444) curve, but there are important differences. In (888) the $\Delta\theta$ range is about three times greater, the maximum reflecting power is an order of magnitude less, and the number of oscillations is almost twice as large as in (444). In (880), with $\gamma_0 > |\gamma_H|$, the $\Delta\theta$ range is reduced eight-fold with respect to (888), while the reflecting power is almost the same as for (444). Yet as shown by the agreement with calculation, both curves correspond to the strain and damage distributions of Fig. 3(b).

The more rapid oscillations of the calculated (888) and (880) curves have larger amplitude than in the experimental curves. The discrepancy is due to the assumption of planar uniformity in the sample and the neglect of incident beam divergence. In (444) the incident beam divergence is much less than the period of oscillation, but in (880), with $\gamma_0 > |\gamma_H|$, they are comparable. The convolution of the plane-wave solution with the incident beam, approximated here as a Gaussian with 6-arc sec standard deviation, produces the calculated curve in Fig. 5(b). The agreement with data is very good. For the (880) reflection with opposite asymmetry, $\gamma_0 < |\gamma_H|$, the incident beam divergence is again negligible compared to the period of oscillation. Although not shown in these figures, the plane-wave calculation, based on the strain and damage of Fig. 3(b), agrees equally well with the data.

The (444) rocking curves of samples FII (double im-

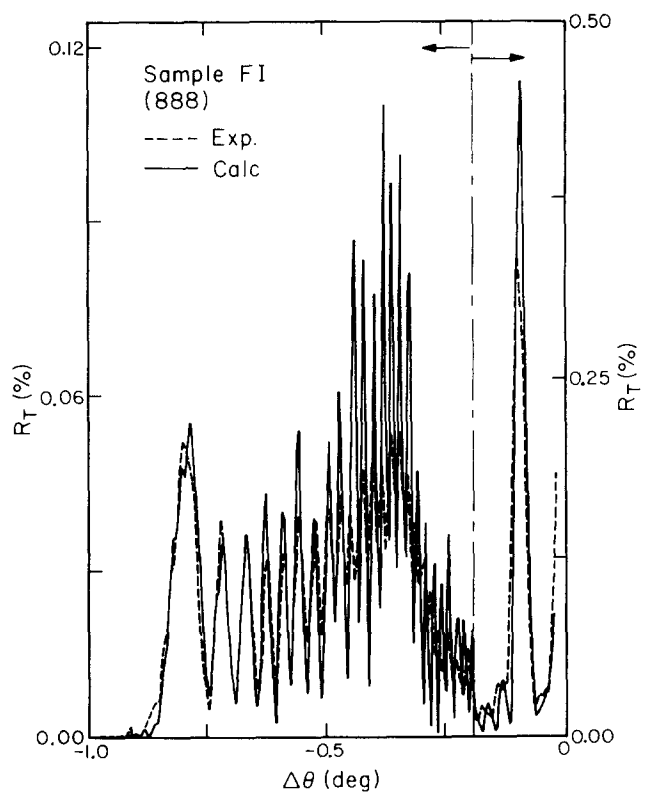

FIG. 4. Experimental (dashed) and calculated (solid) (888) rocking curve of sample FI.

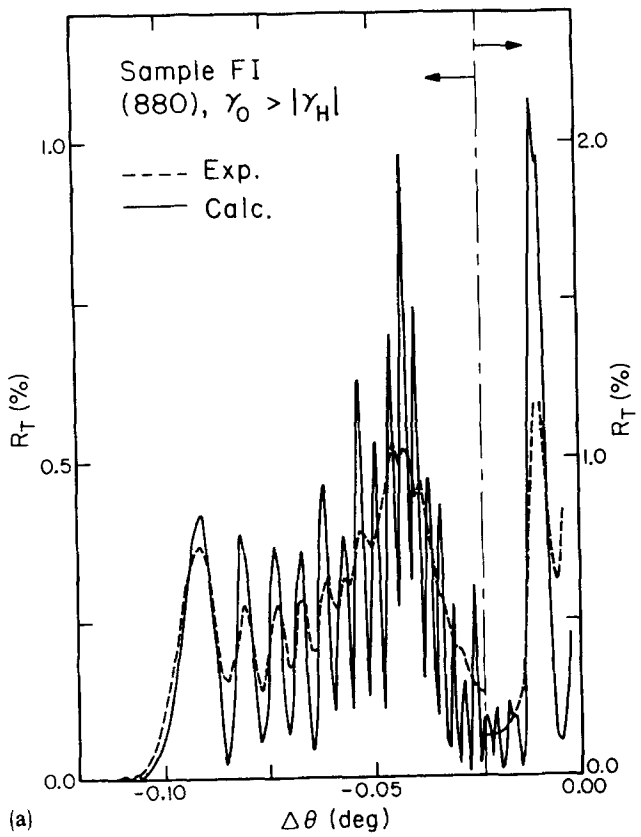

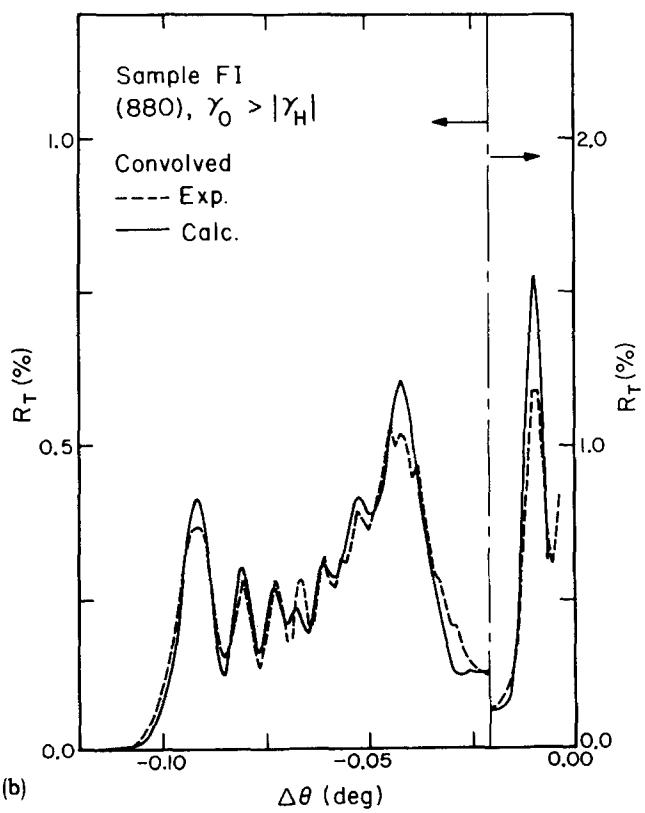

FIG. 5(a) Experimental (dashed) and calculated (solid) (880), $\gamma_0 > |\gamma_H|$, rocking curve of sample FI. (b) Same as (a) after the plane-wave solution was convolved with a Gaussian of 6-arc sec standard deviation.

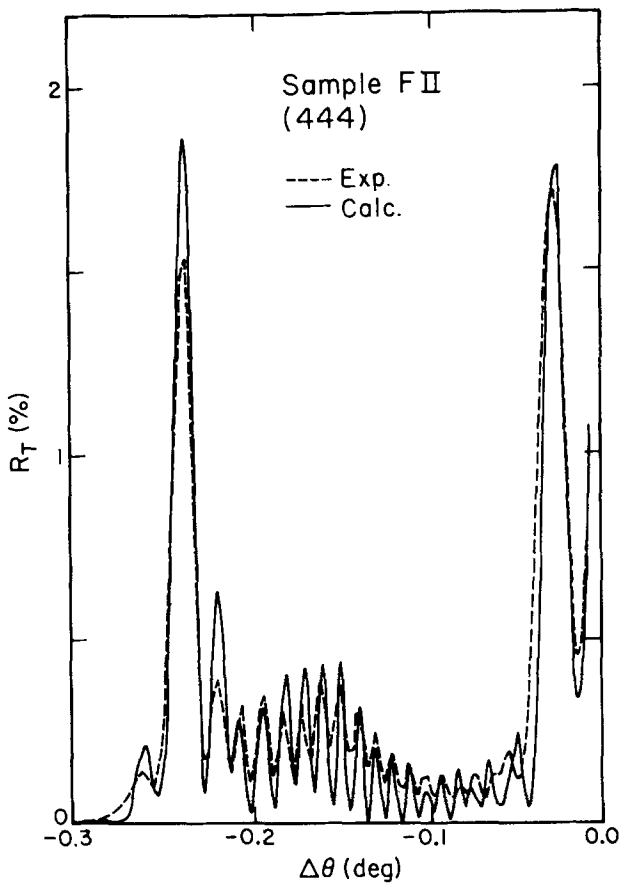

FIG. 6. Experimental (dashed) and calculated (solid) (444) rocking curves of sample FII, implanted with 140 keV, 3×10^{15} He^+/cm^2 + 70 keV, 1.4×10^{15} He^+/cm^2.

planation) and FIII (triple implanation) are shown in Fig. 6 and 7, respectively. The two curves exhibit a continuous change from the FI data [curve 0 in Fig. 3(a)]. The peak at $\Delta\theta \approx -0.24$ deg is becoming sharper and more intense, while the reflecting power in the range -0.22 deg $\lesssim \Delta\theta \lesssim -0.05$ deg is diminishing. The strain distributions corresponding to this behavior are shown in Fig. 8. For clarity, the damage distributions have been omitted. In each case, the relationship between damage and implanation-induced strain is the same as in Fig. 3(b). It is evident that a given depth strain and damage are unaffected by shallower implantation. The rocking curve of another unmilled FIII sample was significantly different from the data in Fig. 7. For that sample the strain distribution was much more uniform, with surface value of $\sim 0.8\%$, instead of the 0.57% shown in Fig. 8.

B. Ne^+-implanted GGG

Experimental and calculated rocking curves of 100-keV Ne^+-implanted GGG are shown in Figs. 9(a)–(e). The doses were 0, 0.5, 1.0, 2.0, and 6.0×10^{14} atoms/cm^2, respectively. The angle axis is the same for all cases, but the reflecting power varies by an order of magnitude. The experimental rocking curve of the virgin sample [Fig. 9(a)] is well enough represented by the dynamical result for nonabsorbing crystals, but no special significance should be attached to this. If

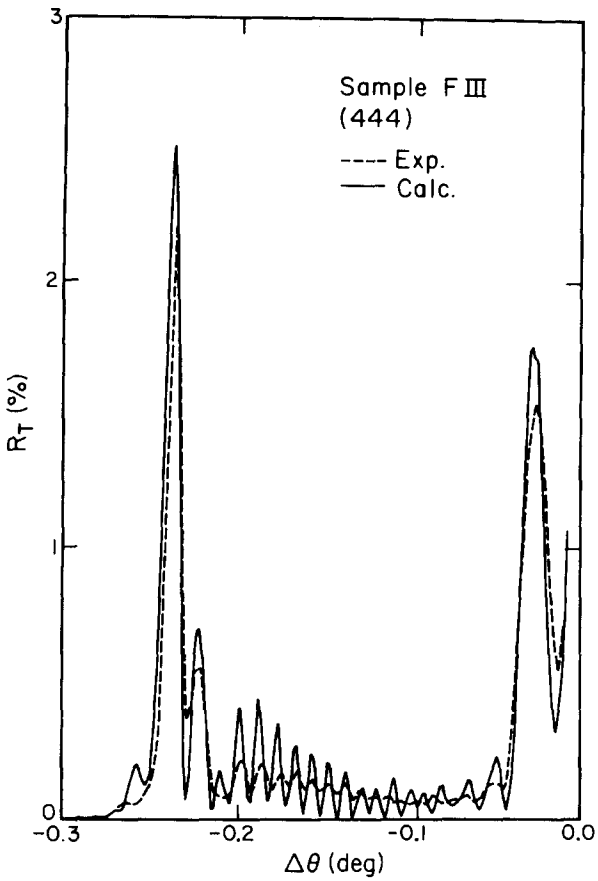

FIG. 7. Experimental (dashed) and calculated (solid) (444) rocking curves of sample FIII, implanted with 140 keV, 3×10^{15} He^+/cm^2 + 70 keV, 1.4×10^{15} He^+/cm^2 + 30 keV, 9×10^{14} He^+/cm^2.

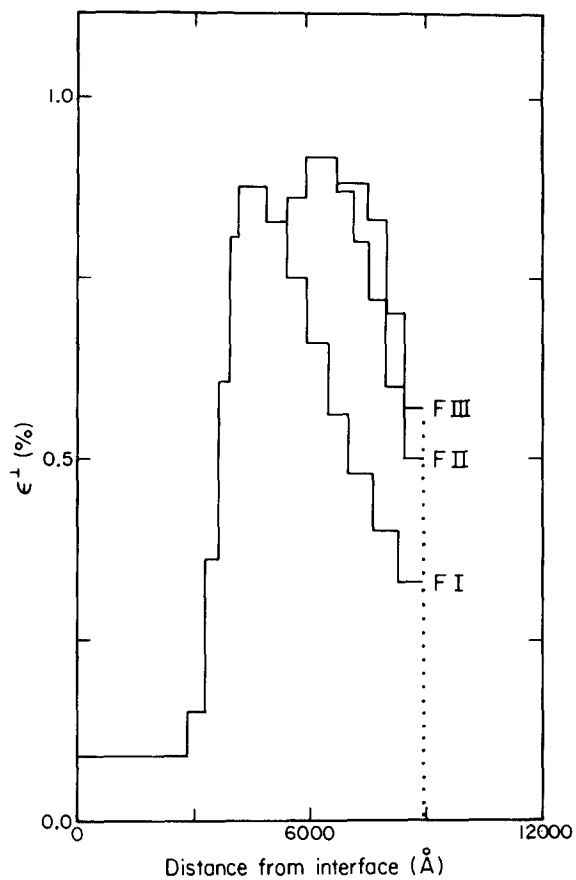

FIG. 8. Strain distributions of samples FI, FII, and FIII.

absorption is taken into account, the dynamical curve is considerably narrower for $\Delta\theta \gtrsim -0.01$ deg and $R_T \lesssim 2\%$. As described in Sec. II, the increased width of the experimental curve is attributed mainly to lattice parameter variations. The dynamical solution for nonabsorbing thick crystals is used throughout this paper to represent the substrate contribution.

The range of nonzero reflecting power in Figs. 9(b), 9(c), and 9(d) increases linearly with dose. At the same time the peak farthest from the origin decreases in relation to other peaks, as does the overall reflecting power. At 6×10^{14} Ne^+/cm^2, Fig. 9(e), the oscillations are much reduced and the reflecting power is close to that of virgin GGG. The calculated curves match the data quite well over the entire range of doses.

The strain and damage distributions corresponding to the calculated curve in Fig. 9(d) are shown in Fig. 10. The layer thickness, maximum strain, and maximum damage are 1900 Å, 2.49% and 0.40 Å, respectively. Damage is linear with strain, with $U_j(\text{Å}) = 0.16\,\epsilon_j^{\perp}(\%)$. As for the He^+-implanted films, some deviation from linearity is possible. The relatively heavy damage level presents the opportunity to demonstrate the importance of including damage in the calculation. Figure 11 shows the same experimental data as Fig. 9(d). The theoretical curve in Fig. 11 was obtained using the strain of Fig. 10 but assuming no damage, i.e., $U_j \equiv 0$ at all depths. The positions of the calculated maxima and minima are unchanged from those in Fig. 9(d), but the integrated reflecting power is now several times greater. In addition, the relative height of the maxima no longer agrees with the data.

The strain and damage distributions obtained for the lower doses, 0.5 and $1.0\times10^{14}/cm^2$, when multipled by 3.4 and 2.0, respectively, are practically identical to those of Fig. 10. The invariance of the shape with dose strongly suggests that strain is linear with dose. This further implies that the ratio 3.4 instead of 4.0 between the 2.0 and $0.5\times10^{14}/cm^2$ distributions is either due to an error in the dose or to annealing effects. The former is considered more likely. The calculated curve in Fig. 9(e) was obtained assuming linearity of strain and damage with dose. The peak strain and damage are then 7.5% and 1.2 Å, respectively. The latter number is close to the interatomic spacing and represents amorphousness. Experimentally and theoretically, most of the implanted layer no longer diffracts. The undulating part of the calculated curve indicates the presence of a thin crystalline region near the interface. The undulation is much reduced in the experimental data, possibly because of sample curvature which increases with strain.

VI. DISCUSSION OF THE RESULTS

The kinematical theory is able to account for the rocking curves of ion-implanted garnets with a wide range of layer thickness, strain, and damage level. Symmetric reflections are sensitive only to strains perpendicular to the sur-

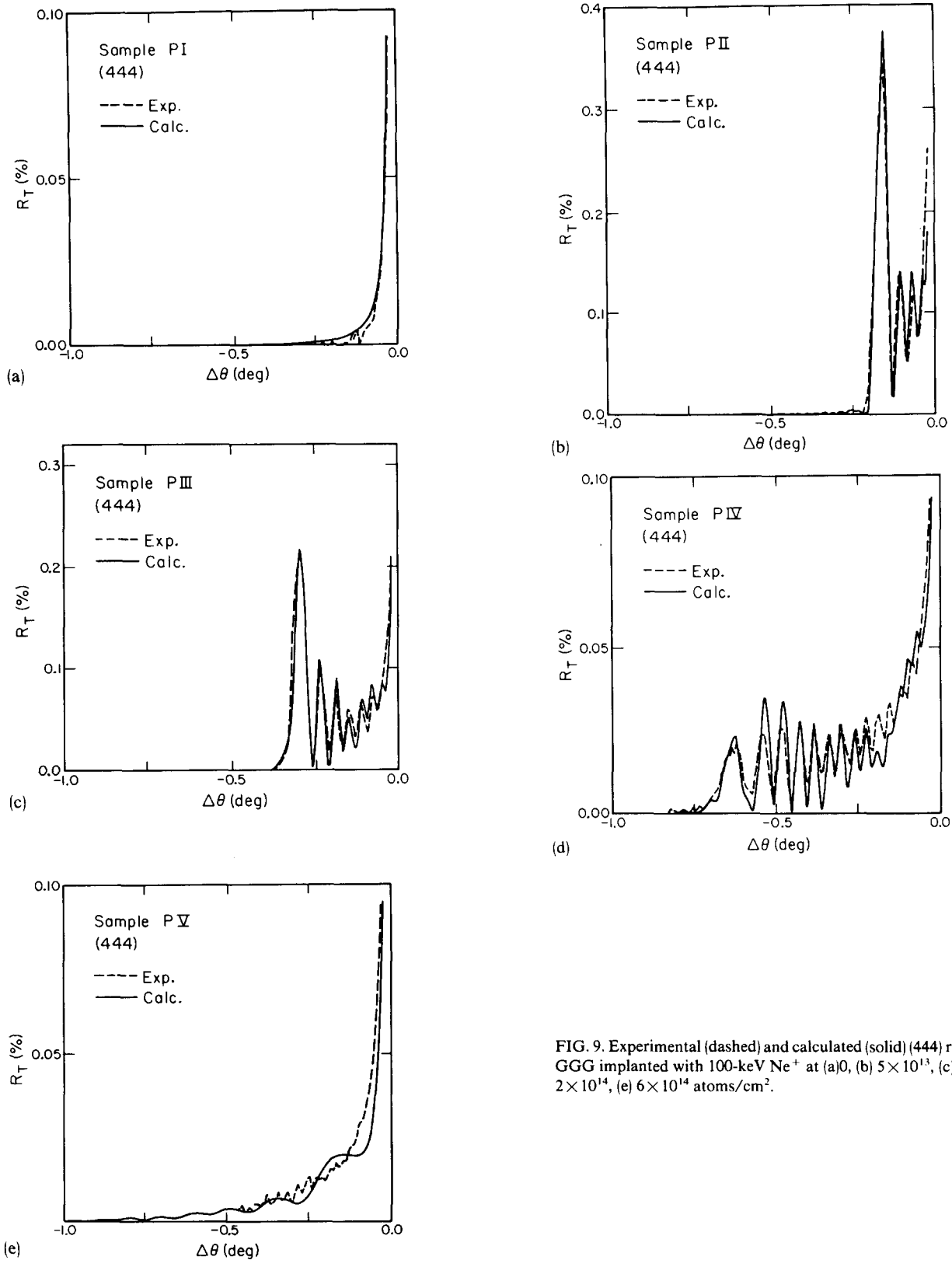

FIG. 9. Experimental (dashed) and calculated (solid) (444) rocking curves of GGG implanted with 100-keV Ne^+ at (a)0, (b) 5×10^{13}, (c) 1×10^{14}, (d) 2×10^{14}, (e) 6×10^{14} atoms/cm^2.

face, while asymmetric reflections measure both perpendicular and lateral strain. The agreement between calculated and experimental curves obtained with asymmetric reflections indicates that the lattice is indeed strained only in a direction perpendicular to the surface. Lateral strain is zero, as expected from the lattice match requirement.

The theoretical reduction in reflecting power due to random atomic displacement is very different for (444), (888), and (880). The good fit to these curves indicates that the assumed spherically symmetric Gaussian $\rho(\Delta\mathbf{r}_j)$ is consistent with the data. However, the validity of this assumption remains unproved. Since garnets are polyatomic, the

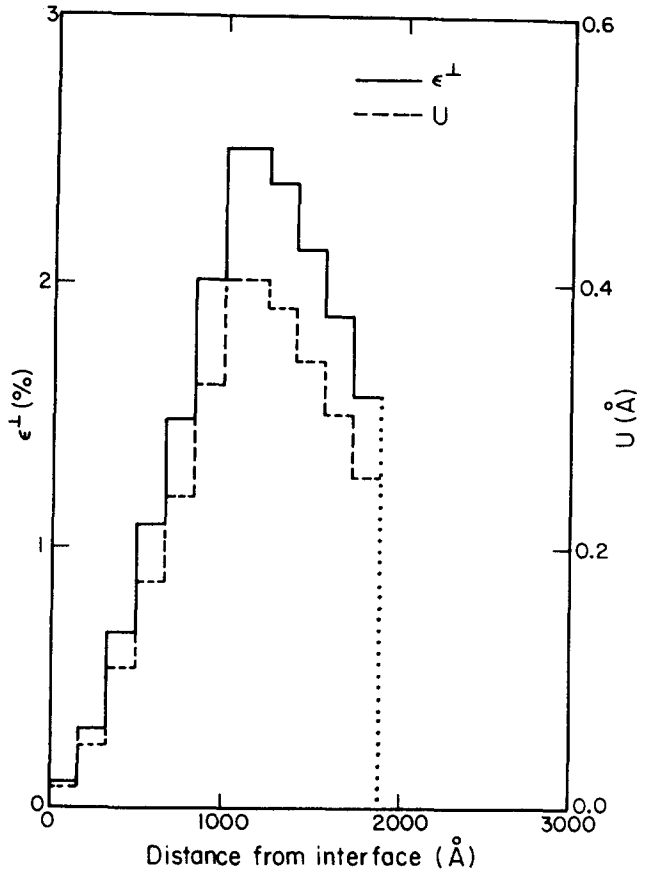

FIG. 10. Strain (solid) and U (dashed) distributions for sample PIV (2×10^{14} Ne^+/cm^2). The same distributions, when scaled by approximately the dose ratios, correspond to all other doses.

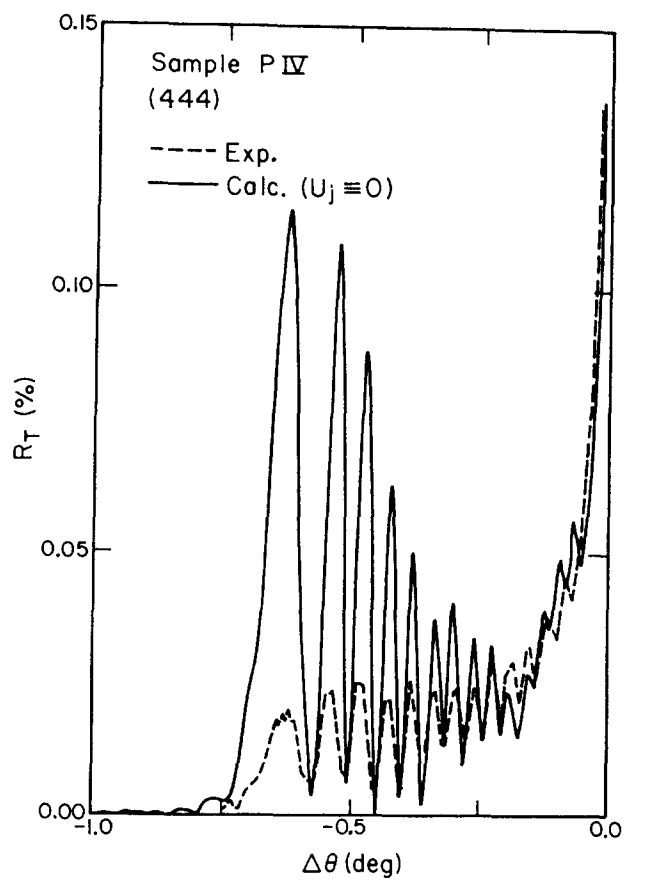

FIG. 11. Experimental (dashed) and calculated (solid) (444) rocking curves of sample PIV. The calculated curve was obtained from strain distribution of Fig. 10, but with zero damage.

contributions of various atoms to the structure factor depend on the particular reflection. It is conceivable that implantation results in a rearrangement of atoms such that the effect on the magnitude of the structure factor is the same as for random displacement. This ambiguity can be reduced by studying several other reflections. For (444), (888), and (880), the relative contribution of c sites, occupied by Gd, Tm, and Y, is $\sim$80, 60, and 60%, respectively. The remaining contribution is almost entirely due to a combination of a sites (Fe) and d sites (Fe and Ga). The most abundant element, O, contributes very little in these reflections. Assuming random displacement, the obtained damage distributions apply mostly to the heavier elements in garnet. In a recent comparison[17] of the kinematical technique and backscattering spectrometry, the damage distributions obtained by the two methods were in satisfactory agreement.

The remarkably large strain and the linearity of the detailed distribution with dose are consistent with earlier results for the maximum strain.[18,19] Because of the lower theoretical sensitivity to damage, strict linearity between damage and strain has not been established. However, the results suggest that both the maximum and the average damage are linear with strain and dose. For both crystals, the proportionality constant between U and $\epsilon^{\perp}$ is 0.17 ± 0.01 Å. This relationship shows that strain and damage are initimately connected. *A priori* it might be expected that strain is due to the incorporation of implanted atoms into the unit cell. Such an affect was observed in doped Si, where the strain was negative and the damage negligible.[4–7] However, in garnets the range distribution of ions is significantly different from the strain distribution.[20] It was shown in Ref. 20 that the detailed strain distribution can be explained entirely in terms of nuclear energy loss. In that study the same strain was obtained with Ne^+ and He^+ doses which differed by almost two orders of magnitude. This was shown to be due to the difference in nuclear energy loss rates for Ne^+ and He^+.

The presence of pronounced oscillations even in the moderately damaged sample PIV indicates that coherence and uniformity are maintained over macroscopic dimensions. In these garnets implantation appears to create only point defects. If extended defects, which cause strain and orientation variations, were present, the oscillatory structure would be smoothed out. Evidence of extended defects accompanied by severe broadening of the rocking curve was presented[12] for garnets subjected to relatively high ($\gtrsim 10^{16}/cm^2$) He^+ doses. In those samples annealing resulted in large defect clusters probably caused by He bubble formation.

VII. SUMMARY

A kinematical model for general Bragg case x-ray diffraction in nonuniform crystals was presented. The kinematical approach has the advantage of computation speed over the more rigorous dynamical theory. The model is valid for

films of arbitrary thickness, provided the maximum reflecting power is less than $\sim 6\%$. This requirement translates to maximum thickness of $\sim 1\ \mu$m for typical crystals such as ion-implanted or doped Si, Ge, GaAs, and garnet. The model incorporates depth-dependent strain and random atomic displacements. Distributions in crystals are obtained by fitting the model to experimental rocking curves. The theoretical rocking curve is shown to be highly sensitive to strain distributions, layer thickness, lateral uniformity, and to a lesser extent, damage distributions. Accuracy of up to $\sim 2\%$ for these parameters is achievable.

The model was applied to He^+-implanted Gd, Tm, Ga:YIG and Ne^+-implanted $Gd_3Ga_5O_{12}$. In the former crystal the total strained layer thickness was 0.89 μm, with the strain varying between 0.09 and 0.91%. The maximum standard deviation U of random atomic displacements was 0.15 Å. Using symmetric and asymmetric reflections, the absence of lateral strain was demonstrated. In addition, the assumption of spherically symmetric random displacements was consistent with the data. The $Gd_3Ga_5O_{12}$ crystal was implanted with several doses corresponding to a wide range of damage. In all cases the layer thickness was 1900 Å; strain values of 2.49% corresponded to 0.40-Å U values. The detailed strain distribution was strictly proportional to ion dose. The damage distribution was closely linear with implantation-induced strain, although some deviation from strict linearity has not been ruled out. Both crystals showed the same relationship between damage and strain. The GGG crystal maintained single crystallinity up to the amorphous threshold.

ACKNOWLEDGMENTS

Thanks are due to C. H. Wilts for his continued support and for a careful reading of the manuscript. The contribution of H. L. Glass in the form of helpful discussions is gratefully acknowledged. B. M. Paine is thanked for the ion implantation of the GGG samples. Technical assistance by L. A. Moudy is acknowledged.

[1]S. Takagi, Acta Crystallogr. **15**, 1311 (1962).
[2]D. Taupin, Bull. Soc. Fr. Miner. Crist. **87**, 469 (1964).
[3]S. Takagi, J. Phys. Soc. Jpn. **26**, 1239 (1969).
[4]J. Burgeat and D. Taupin, Acta Crystallogr. A **24**, 99 (1968).
[5]J. Burgeat and R. Colella, J. Appl. Phys. **40**, 3505 (1969).
[6]A. Fukuhara and Y. Takano, Acta Crystallogr. A **33**, 137 (1977).
[7]B. C. Larson and J. F. Barhorst, J. Appl. Phys. **51**, 3181 (1980).
[8]R. W. James, *The Optical Principles of the Diffraction of X-rays* (Cornell University, Ithaca, New York, 1965).
[9]A. M. Afanasev, M.V. Kovalchuk, E. V. Kovev, and V. G. Kohn, Phys. Status Solidi A **42**, 415 (1977).
[10]See, for example, M. Buerger, *Vector Space and Its Application in Crystal-Structure Investigation* (Wiley, New York, 1953).
[11]V. S. Speriosu, H. L. Glass, and T. Kobayashi, Appl. Phys. Lett. **34**, 539 (1979).
[12]V. S. Speriosu, B. E. MacNeal, and H. L. Glass, Intermag. 1980 Conf., Boston, paper 22-4 (unpublished).
[13]W. H. Zachariasen, *Theory of X-ray diffraction in Crystals* (Wiley, New York, 1945).
[14]The Gd, Tm, Ga: YIG films and the ion milling were provided by the San Jose, California laboratory of IBM Corporation.
[15]K. Ju, R. O. Schwenker, and H. L. Hu, Intermag. 1979, New York (unpublished).
[16]Virgin GGG wafers were provided by the Anaheim, California laboratory of Rockwell International.
[17]B. M. Paine, V. S. Speriosu, L. S. Wieluński, H. L. Glass, and M-A. Nicolet, Fifth International Conf. Ion Beam Analysis, Sydney, Australia, 1981; Nucl. Instr. Meth. (in press).
[18]J. C. North and R. Wolfe, "Ion-Implantation Effects in Bubble Garnets" *In Ion-Implantation in Semi-conductors and Other Materials*, edited by B. L. Crowder (Plenum, New York, 1973).
[19]K. Komenou, I. Hirai, K. Asama, and M. Sakai, J. Appl. Phys. **49**, 5816 (1978).
[20]B. E. MacNeal and V. S. Speriosu, J. Appl. Phys. **52**, 3935 (1981).